Available online at www.sciencedirect.com

ScienceDirect

Procedia Structural Integrity 24 (2019) 724–737

Structural Integrity Procedia

www.elsevier.com/locate/procedia

AIAS 2019 International Conference on Stress Analysis

Optimisation of industrial parts by mesh morphing enabled automatic shape sculpting

Stefano Porziani[a,*], Corrado Groth[a], Luca Mancini[a], Riccardo Cenni[b], Matteo Cova[b], Marco Evangelos Biancolini[a]

[a] *University of Rome "Tor Vergata", Rome 00133, Italy*
[b] *Sacmi Imola S.C., Via Prov.le Selice 17/a, Imola 40026, Italy*

Abstract

Radial basis functions (RBF) mesh morphing is a well established approach to quickly update an existing finite element analysis (FEA) mesh so that new shapes can be adapted and related performances explored. The RBF in fact allow to adapt the volume mesh maintaining a good quality even for substantial changes of the shape. New shapes imposed at FEA domain borders can be controlled by direct parameters (mesh based or CAD based) or by deformation fields resulting from the physics. In this paper we explore how the last approach can be exploited according to two different strategies: the biological growth method (BGM), which consists in adding/removing material according to the local stress at surface, the adjoint method, which consists in moving inward outward the surface according to the surface sensitivities.

The FEA solver ANSYS® Mechanical™ in combination with the mesh morphing software RBF Morph™ was adopted for this purpose. The BGM implementation is the one implemented in RBF Morph, the adjoint solver is the one implemented in the topological optimisation tool by ANSYS.

Automatic shape sculpting applications are demonstrated on a simple geometry, a thick plate with simple load conditions, and on an industrial part.

Keywords: FEA; RBF; Structural automatic optimisation; Biological Growth Method; Mesh morphing

1. Introduction

In industrial production and design, optimisation can be the key to success for a product. Through optimisation of the product, an enterprise can maximise earnings by limiting costs and raw material usage. Optimisation tasks can be very challenging, because while seeking for an optimal component configuration, designers have to maintain its compliance to the task it is designed for (e.g. strength and functionality requirements). In last years numerical

* Corresponding author. Tel.: +39-06-7259-7136.
E-mail address: porziani@ing.uniroma2.it

10.1016/j.prostr.2020.02.064

simulations provided a valuable tool to virtually test several configurations in order to verify performances indexes and shorten time needed for the identification of the optimal one. The Finite Element Method (FEM) is widespread adopted to accomplish the optimisation task: a virtual numerical model reproduces not only shapes of the real component, but also loads and constraints representing real working conditions. The main drawback of this approach is that for each geometrical variation a new FEM model is required to be built and, specially with complex geometries, this task can become time-consuming.

A valuable alternative to model regeneration (a task that includes both geometrical description of the component and the model remeshing)is mesh morphing (de Boer et Al. (2007), Biancolini (2011) and Staten et Al. (2011)). This technique allows the user to modify model nodes positions with no need to re-mesh and to re-execute model set up (i.e. material, load and constraint definition). This method proved to be a valuable tool not only in computational structural mechanics (CSM) and computational fluid-dynamics (CFD), but also in other engineering applications (such as ice accretion simulations as in Biancolini and Groth (2014)).

Biancolini and Cella (2010) used mesh morphing to study an aeroelastic application that can be tackled adopting pressure mapping methods (Biancolini et Al. (2018)) or modal shapes embedding (Groth et Al. (2019)); mesh morphing allowed also to perform shape parameterisation in an optimisation study (Cella et Al. (2017)). In Biancolini et Al. (2018) mesh morphing was successfully adopted in the parameterisation and study of crack shapes: in the cited work authors proposed an automatic procedure to simulate the crack growth and propagation; the same approach was then proven for the case of near-surface defects (Dai et Al. (1998)) in the study by Giorgetti et al. (2018).

Mesh morphing was also successfully coupled with an adjoint solver in Groth et Al. (2018): exploiting adjoint information on model surfaces, stress levels were successfully optimised in an gradient based optimisation procedure characterised by high computational and optimisation efficiency.

Recently mesh morphing was successfully coupled with an innovative optimisation approach, the biological growth method (BGM). This method mimics the behaviour of biological tissues which grow where a surface stress concentration arises. In Porziani et Al. (2018) the authors used BGM, driving the shape optimisation according to surface stress levels and applying them according to a traditional manufacturing process.

In the present work the mesh morphing technique is applied to industrial components optimisation driving the shape modification using both the BGM method and adjoint sensitivities on component surfaces, with different optimisation goals. Numerical simulations are performed in the framework of ANSYS Workbench™ finite element analysis (FEA) tool, using RBF Morph mesh morpher based on radial basis functions (RBFs). BGM data are evaluated inside RBF Morph, whilst adjoint sensitivities are evaluated using ANSYS Topology Optimisation tool.

1.1. The Biological Growth Method

The Biological Growth Method (BGM) can be described as a shape optimisation method based on surfaces stress levels. The method replicates the behaviour of biological structures as tree trunks and animal bones, which evolve by adding biological material at surface locations where an activation stress level is located. Heywood (1969) and Mattheck et Burkhardt (1990) extended this concept in reverse direction: material can also be removed from surfaces locations if stresses are lower than a certain level. Thanks to photoelastic techniques Heywood (1969) proved that it is possible to reach a uniform stress distribution along the boundary of a stress raiser if the boundary shape is modified according to BGM method. Mattheck et Burkhardt (1990) presented a 2D study capable to predict the shape evolution observed in natural structures: this approach was applied in CAE based optimisation of a plate with a circular hole and with a chain link. Authors computed the volumetric growth ($\dot{\varepsilon}$) proposing a relationship between the von Mises stress (σ_{Mises}) and a threshold stress (σ_{ref}). According to authors, threshold stress has to be chosen depending on the allowable stress for the specific design (1).

$$\dot{\varepsilon} = k\left(\sigma_{Mises} - \sigma_{ref}\right) \tag{1}$$

In Waldman and Heller (2015) a more complex model for layer addition was proposed, in order to be applied in optimisation of holes in air-frame structure, when multiple stress peak location are identified. Proposed formula is reported in (2):

$$d_i^j = \left(\frac{\sigma_i^j - \sigma_i^{th}}{\sigma_i^{th}} \right) \cdot s \cdot c \,, \qquad \sigma_i^{th} = max(\sigma_i^j) \text{ if } \sigma_i^j > 0 \quad \text{or} \quad \sigma_i^{th} = min(\sigma_i^j) \text{ if } \sigma_i^j < 0 \tag{2}$$

The more complex model allow to move the i-th boundary node of the j-th region by a distance d_i^j, computed using (2), where σ_i^j is the principal stress on the plane tangent to the surface to be modified, σ_i^{th} is the stress threshold, c is and arbitrary characteristic length and s is a step size scaling factor.

In the present work an improved implementation of BGM is used that is available as a standard feature of RBF Morph software, as illustrated in Biancolini (2018). The implemented algorithm defines the node displacement ($S_{node\ BGM}$) in the direction normal to the surface, amplitude of displacement is evaluated using (3), where σ_{node} is the stress evaluated at each node, σ_{th} is a threshold value for stress defined by user, σ_{max} and σ_{min} are respectively the maximum and the minimum stress value identified in the analysed nodes set. In order to limit the mesh distortion, which in mesh morphing can occur, the parameter d is defined as the maximum offset between the nodes on which the maximum stress is identified and the nodes on which the minimum stress is identified. The d parameter is defined by the user: low values require more BGM iterations to evolve the shape, high values could lead to distorted shapes; a trade-off should be set according to experience and best practices.

$$S_{node\ BGM} = \frac{\sigma_{node} - \sigma_{th}}{\sigma_{max} - \sigma_{min}} \cdot d \tag{3}$$

With this implementation, nodes can be moved either inward and in outward direction if stress on each node is lower or higher than the defined threshold value respectively.

The BGM implementation available in RBF Morph allows the user to perform shape optimisation according to different equivalent stresses and strains, as reported in Table 1.

Table 1. Stress and strain types available in the RBF Morph implementation of BGM.

Stress/Strain type	Equation
von Mises stress	$\sigma_e = \sqrt{(\sigma_1 - \sigma_2)^2 + (\sigma_2 - \sigma_3)^2 + (\sigma_3 - \sigma_1)^2}$
Maximum Principal stress	$\sigma_e = max(\sigma_1, \sigma_2, \sigma_3)$
Minumum Principal stress	$\sigma_e = min(\sigma_1, \sigma_2, \sigma_3)$
Stress intensity	$\sigma_e = max(\lvert\sigma_1 - \sigma_2\rvert, \lvert\sigma_2 - \sigma_3\rvert, \lvert\sigma_3 - \sigma_1\rvert)$
Maximum Shear stress	$\sigma_e = 0.5 \cdot (max(\sigma_1, \sigma_2, \sigma_3) - min(\sigma_1, \sigma_2, \sigma_3))$
Equivalent Plastic strain	$\varepsilon_e = [2(1+\nu')]^{-1} \cdot \left(0.5\sqrt{(\varepsilon_1 - \varepsilon_2)^2 + (\varepsilon_2 - \varepsilon_3)^2 + (\varepsilon_3 - \varepsilon_1)^2}\right)$

1.2. Overview of adjoint method for structural problems

Adjoint methods allow to obtain with a single evaluation the sensitivities of an objective function with respect to a set of parameters. The sensitivity of the performance can be evaluated in the three direction for each mesh node, allowing to obtain the influence of a given shape parameterisation (Papoutsis-Kiachagias et al. (2015), Papoutsis-Kiachagias et al. (2016)) or a new one (Groth (2015)). Adjoint methods are widespread used in fluid dynamics applications (Nadarajah and Jameson (2001), Newman and Taylor (1999)), but can successfully applied in CSM applications, working directly on problem describing physics. It is possible either to differentiate the discretised equa-

tions of finite elements ((Brockman and Lung (1988), Yatheendharr and Belegundu (1993), Francavilla et al. (1975)), or to derive the equations prior to their differentiation (Dems and Mroz (1983), Dems and Haftka (1988)); these approaches are called, respectively, discrete adjoint method and continuous adjoint method. In the case of the discrete method the optimisation can be driven by an objective function in the form:

$$\Psi = f(\mathbf{X}(u), u) \tag{4}$$

in which the independent variable X is the structural displacement and the function 4 is directly and indirectly influenced by parameter u. Its variation in function of this parameter can be expressed as:

$$\frac{d\Psi}{du} = \frac{\partial\Psi}{\partial u} + \frac{\partial\Psi}{\partial\mathbf{X}}\frac{\partial\mathbf{X}}{\partial u} \tag{5}$$

Terms $\frac{\partial\Psi}{\partial u}$ and $\frac{\partial\Psi}{\partial\mathbf{X}}$ reported in 5 can be easily evaluated knowing the analytic expression of Ψ. The last therm, $\frac{\partial\mathbf{X}}{\partial u}$, can be evaluated via the direct method or the adjoint method. Consider for example the static problem that can be described by the equation:

$$\mathbf{K}\mathbf{X} = \mathbf{F} \tag{6}$$

For this problem, the variation with respect to parameter u is:

$$\mathbf{K}\frac{\partial\mathbf{X}}{\partial u} + \mathbf{X}\frac{\partial\mathbf{K}}{\partial u} = \frac{\partial\mathbf{F}}{\partial u} \tag{7}$$

This equation can be rearranged in the following form:

$$\mathbf{K}\frac{\partial\mathbf{X}}{\partial u} = \frac{\partial\mathbf{F}}{\partial u} - \mathbf{X}\frac{\partial\mathbf{K}}{\partial u}. \tag{8}$$

Similarly to (6), it is possible to consider (8) as the equation of a static problem structure with stiffness $\mathbf{K}$ but this time subject to a fictitious load equal to $\frac{\partial\mathbf{F}}{\partial u} - \mathbf{X}\frac{\partial\mathbf{K}}{\partial u}$. It is possible to obtain the displacement field $\frac{\partial\mathbf{X}}{\partial u}$ that can be employed to solve equation (5), obtaining:

$$\frac{d\Psi}{du} = \frac{\partial\Psi}{\partial u} + \frac{\partial\Psi}{\partial\mathbf{X}}\mathbf{K}^{-1}\left(\frac{\partial\mathbf{F}}{\partial u} - \mathbf{X}\frac{\partial\mathbf{K}}{\partial u}\right) \tag{9}$$

The procedure described above is the direct method for structural sensitivity calculation. In case it is necessary to evaluate sensitivities with respect to more than one parameter, a new calculation for each additional parameter has to be performed.

In the adjoint method we add an additional variable with respect to the direct method, the adjoint variable, that can be seen as a Lagrange multiplier (Belegundu (1985)) of the constraint (6) in the Lagrangian built together with (4).

The adjoint variable, multiplied for the stiffness matrix, allows to obtain the adjoint equation:

$$\mathbf{K}\lambda = \frac{\partial \Psi^{\mathrm{T}}}{\partial \mathbf{X}} \tag{10}$$

That is the same structure of (6) with a fictitious load equal to $\frac{\partial \Psi}{\partial \mathbf{X}}^{\mathrm{T}}$. Obtained displacements are then employed in (9) obtaining the following equation:

$$\frac{d\Psi}{du} = \frac{\partial \Psi}{\partial u} + \lambda^{\mathrm{T}} \left(\frac{\partial \mathbf{F}}{\partial u} - \mathbf{X} \frac{\partial \mathbf{K}}{\partial u} \right). \tag{11}$$

Using the adjoint method allows to perform only one calculation, no matter how many parameter are used, because (10) is not dependent from parameter u, but only form Ψ.

Direct and adjoint methods are then efficient depending on the case: if the number m of objective functions Ψ is greater than the number p of parameters u ($m \gg p$), the direct method is advisable, whilst if the number p of parameters u is greater than the number m of objective functions Ψ ($m \ll p$), then the adjoint method is preferable. Dealing with shape optimisation, having thus three parameters for each node involved in the optimisation, the adjoint method is the best option

For the applications illustrated in this work, the adjoint data used to drive the shape modification are obtained from the ANSYS Topology Optimisation tool, which is based on the theory described above. The adjoint sensitivities are computed by this tool in the form of a nodal topological density (ρ), a parameter that is defined in the range [0; 1] and which define if the surface around each node has to be moved inward or outward to meet the objective function requirement.

1.3. Recalls on Radial Basis Functions

RBFs are mathematical functions used since 60s as interpolation tools for scattered data (Davies (1963)). An exhaustive examination of RBF theory and method can was given in Porziani et Al. (2018). An RBF used to interpolate scattered scalar values at source points $\boldsymbol{x}_{k_i}$ in the space $\mathbb{R}^n$ can be expressed as in (12).

$$s(\boldsymbol{x}) = \sum_{i=1}^{N} \gamma_i \varphi \left(\left\| \boldsymbol{x} - \boldsymbol{x}_{k_i} \right\| \right) + h(\boldsymbol{x}) \tag{12}$$

$\boldsymbol{x}$ are the points at which the function is evaluated (the target points). φ is the RBF: a scalar function of the Euclidean distance between each source point and the target point considered. γ_i are the weights of the radial basis which are to be evaluated by solving a linear system of equations and N is the number of points to be processed. Several RBF can be adopted: typical RBF are shown in Table 2, in which $r = \left(\left\| \boldsymbol{x} - \boldsymbol{x}_{k_i} \right\| \right)$. In (12) the polynomial h is added to guarantee the existence and uniqueness of the interpolation function.

RBFs can be applied to mesh-morphing to evaluate a vector field of displacement: this can be realised by interpolating separately each displacement component:

$$\begin{cases} s_x(\boldsymbol{x}) = \sum_{i=0}^{N} \gamma_i^x \varphi\left(\|\boldsymbol{x} - \boldsymbol{x}_i\|\right) + \beta_1^x + \beta_2^x x + \beta_3^x y + \beta_4^x z \\ s_y(\boldsymbol{x}) = \sum_{i=0}^{N} \gamma_i^y \varphi(\|\boldsymbol{x} - \boldsymbol{x}_i\|) + \beta_1^y + \beta_2^y x + \beta_3^y y + \beta_4^y z \\ s_z(\boldsymbol{x}) = \sum_{i=0}^{N} \gamma_i^z \varphi(\|\boldsymbol{x} - \boldsymbol{x}_i\|) + \beta_1^z + \beta_2^z x + \beta_3^z y + \beta_4^z z \end{cases} \tag{13}$$

In a mesh morphing RBF problem, source points are the nodes on which the user prescribes the known displacement. It is worth to remark that the effects of the morphing action on the whole domain (numerical model) can be limited by imposing a zero displacement to nodes that wrap the interested area or volume.

Table 2. Most common RBFs.

RBF type	Equation
Spline type (Rn)	$r^n,\ n\ odd$
Thin plate spline	$r^n log(r),\ n\ even$
Multiquadric (MQ)	$\sqrt{1+r^2}$
Inverse multiquadric (IMQ)	$\frac{1}{\sqrt{1+r^2}}$
Inverse quadric (IQ)	$\frac{1}{1+r_2^2}$
Gaussian (GS)	e^{-r^2}

1.4. Automatic surface sculpting

The overall optimisation procedure can be accomplished by connecting the adjoint and BGM data from numerical simulation with the mesh morphing tool RBF Morph. Thanks to this tool, it is possible to prescribe on surface nodes two kind of offset: a fixed surface offset and a driven surface offset (see Fig. 1). In both cases the software can identify the surface normal evaluated at the node position and can use it to impose the node a normal displacement, inward or outward. Through the fixed value surface offset, the nodes on the model surface will be translated by the same value, along the local surface normal.

By using the driven value surface offset, it is possible to define for each surface node a movement along the surface normal direction, whose intensity is defined according to a sculpting function defined on the node itself. When using a sculpting function based on the BGM approach, equation 3 is used by defining the stress/strain type (see Table 2), the threshold value σ_{th} and parameter d. If adjoint approach is used to drive the surface sculpting data from topology optimisation tool is used. This data consists of a nodal topological density ρ, which is defined in the range [0; 1] and is used to decide if a the node has to be maintained or removed from the topologically optimised component. This data can be used considering that if a node has to be removed, the surrounding surface can be moved inward to obtain the same effect. Nodal topological density data can be then used by interpolating it and using it to define the sculpting function. In case the interpolating function is an irrational function (see Fig. 2), the sculpting function is defined as

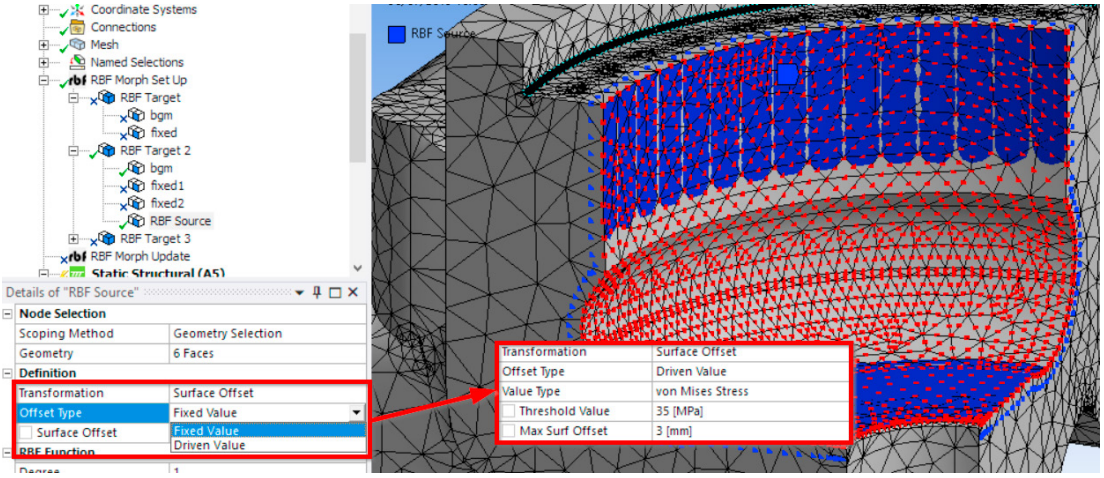

Fig. 1. Surface offset options available with RBF Morph mesh morphing tool

in equation 14, where $S_{node\ adj}$ is the nodal displacement normal to the surface and d is the maximum displacement defined by the user.

$$S_{node\ adj} = \left[0.5\left(\frac{(\rho - 0.5)}{0.5}\right)^{\frac{1}{3}} + 0.5\right] \cdot d, \qquad with\ \rho \in [0,1] \tag{14}$$

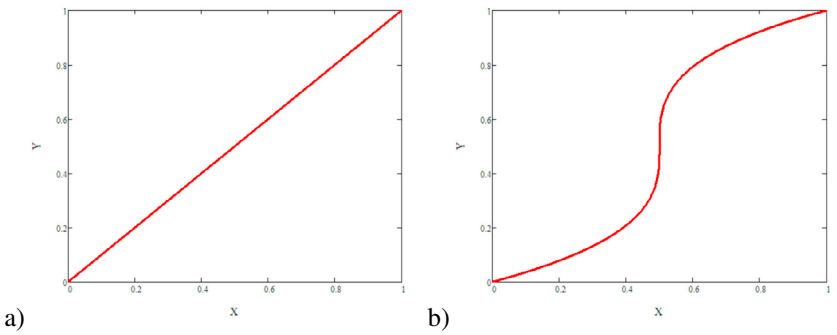

Fig. 2. Function used to interpolate sensitivity data: a) linear function, b) irrational function

2. Applications description

In this section two applications of the proposed optimisation procedure are presented. As stated before, numerical models of these application were realised adopting ANSYS Mechanical as FEM tool (pre-processor, solver and post-processor); the adjoint data adopted to drive the mesh morphing shape update came from ANSYS Topology Optimisation tool; BGM procedure and mesh morphing procedure were managed by RBF Morph ACT Extension for Mechanical.

2.1. Simple thick plate

In order to understand the approach simple mock-up applications are very useful. For simple cases of BGM the reader can refer to Porziani et Al. (2018). In this paper the first illustrative example, whose aim is the illustration of the functionality of adjoint method coupled with RBF based mesh morphing, is a simple thick plate, as depicted in Fig. 3a.

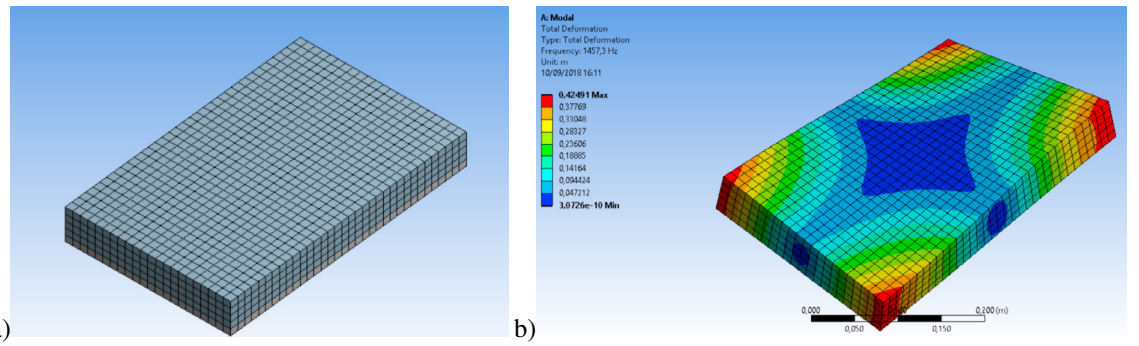

Fig. 3. Simple thick plate: a) geometry, b) first mode shape

The plate is realised using the material properties in ANSYS Mechanical for structural steel and natural modes of the free and un-damped structure are extracted with a normal modes eigenvalues analysis. The first mode shape and first six natural frequencies are reported respectively in Table 3 and Fig. 3b.

Table 3. Simple thick plate natural frequencies

Mode n.	Frequency [Hz]
1	1457.3
2	1542.3
3	3159.1
4	3799.8
5	3816.2
6	4514.7

2.2. Industrial component

In the second application presented in this work, an industrial component is analysed and the optimised. The baseline configuration of this component is depicted in Fig. 4. Since the confidentiality of this industrial component the authors are not allowed to give detailed information about dimensions, loading and constraint conditions and material characteristics.

The optimisation strategies tried to minimise the stress values in the zone identified by number 2 by applying shape modification in zone identified by label 1 in Fig. 5.

3. Simple thick plate optimisation

For the simple thick plate optimisation set-up, the main goal were:

- obtaining a first natural frequency higher than 1220 Hz;
- around 50% overall mass decrease.

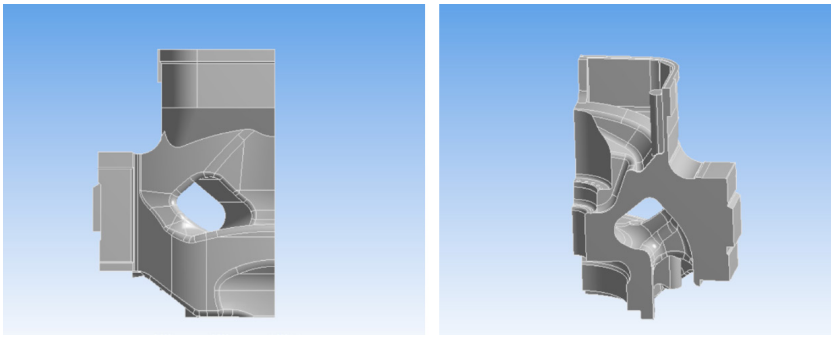

Fig. 4. Industrial component geometries

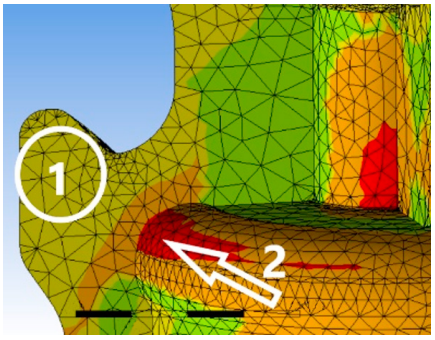

Fig. 5. Industrial component optimisation zones

The topological optimisation tool gave as result the shape reported in Fig. 6, which is based on the nodal topological density ρ.

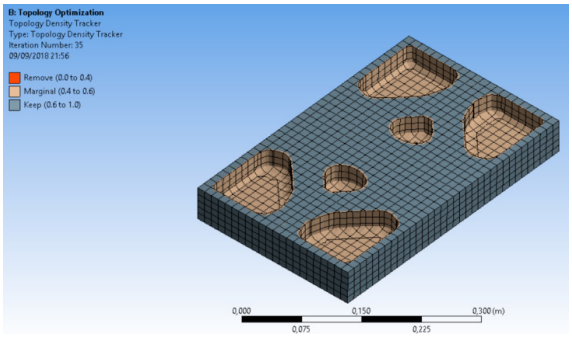

Fig. 6. Simple thick plate optimised by topological optimisation tool

According to what explained in section 1.4, nodal topological density has been interpolated using the linear and irrational interpolation functions (see Fig. 2) and using a d parameter value equal to 15 mm, the resulting optimised shapes are reported in Fig. 7a and Fig. 7b respectively.

Result obtained with optimised model are depicted in Fig. 8 and summarised in Table 4. The first optimisation requisite (first natural frequency higher than 1220 Hz) is satisfied using both interpolation functions. Regarding the 50% mass reduction, it has to be noted that using the linear interpolation for nodal topological density the decrease is around 20%, whilst using the irrational interpolation the mass decrease is around 17%. This is due to the fact that, whilst with the topological optimisation, which effectively removes elements, and consequently material, the 50%

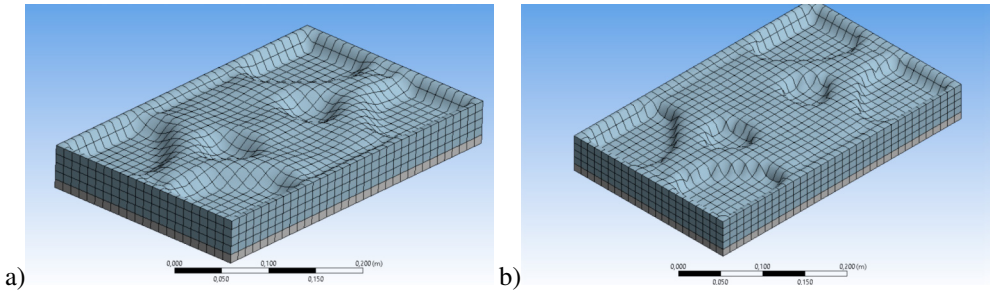

Fig. 7. Simple thick plate optimisation results: a) using linear interpolation; b) using irrational interpolation

mass reduction a realisable target, with the adjoint driven surface sculpting the nodes are only moved, no element is effectively eliminated and the mass reduction amount is therefore lower than the expected value.

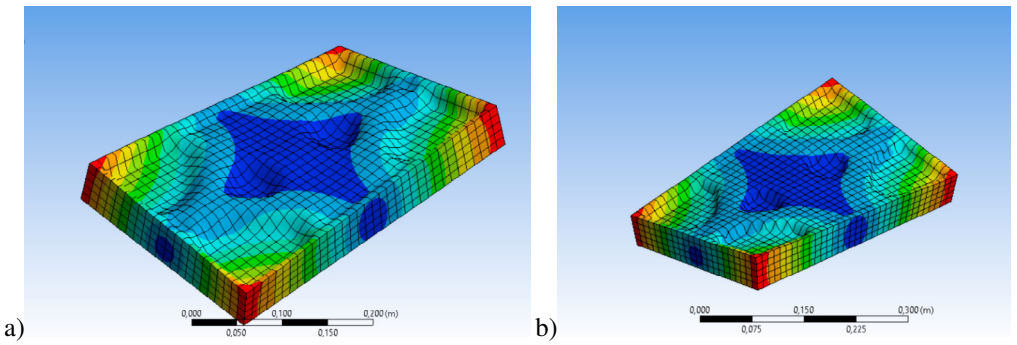

Fig. 8. Simple thick plate optimised first mode shape: a) using linear interpolation; b) using irrational interpolation

Table 4. Simple thick plate result comparison

Mode n.	Baseline Frequency [Hz]	Linear interpolation frequency [Hz]	Irrational interpolation frequency [Hz]
1	1457.3	1315.6	1351.5
2	1542.3	1402.2	1440.7
3	3159.1	2579.7	2616.5
4	3799.8	3238.1	3273.3
5	3816.2	3314.0	3344.7
6	4514.7	3820.0	3874.0

4. Industrial component optimisation

4.1. Adjoint driven surface sculpting

Results for the adjoint driven mesh morphing optimisation applied to the industrial component are here presented. The applied method allowed to obtain interesting results in terms of mass reduction aiming at maintaining unchanged the stress levels. Acting on the component zone highlighted in Fig. 9a, the mesh morphing driven by topological optimisation tool adjoint data allowed to obtain a stress reduction of 11.7% in terms of maximum stress.

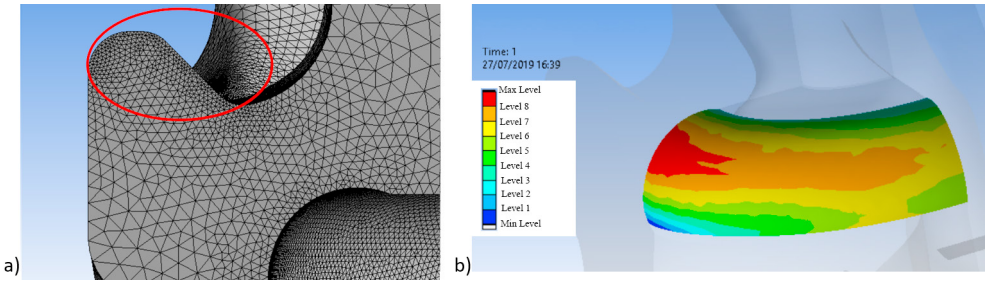

Fig. 9. Industrial component zone 2: a) morphed mesh zone; b) resulting stress distribution

4.2. BGM driven surface sculpting

On the industrial component, also the BGM optimisation approach was applied. With this approach, the aim was to decrease stresses at specific hotspot locations in an automatic way. The procedure was applied on three different stress hotspots, which are represented in Fig. 10 on the industrial component geometry.

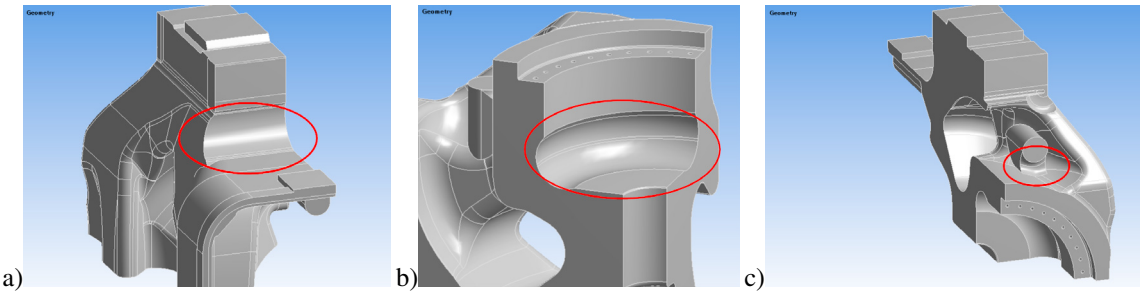

Fig. 10. Industrial component zone 6: a) stress hotspot 1; b) stress hotspot 2; c) stress hotspot 3

According to what illustrated in section 1.1, for each hotspot the BGM set-up was realised using the values for σ_{th} and d reported in Table 5.

Table 5. Parameter set-up for BGM optimisation

Location	σ_{th}	d [mm]
Hotspot 1	$0.5 \cdot (\sigma_{max} + \sigma_{min})$	3
Hotspot 2	$0.5 \cdot (\sigma_{max} + \sigma_{min})$	3
Hotspot 3	$0.5 \cdot (\sigma_{max} + \sigma_{min})$	1

The entire BGM procedure has been iterated 6 times, allowing to obtain stress reduction at specified hotspots. In Fig. 11, Fig. 13 and Fig. 15 the baseline mesh configuration for the three hotspots is compared with the optimised mesh configuration: a geometrical surface, highlighted in green, is reported to ease the comparison.

The stress concentrations at the three hotspot were reduced by the BGM automatic procedure, as depicted in Fig. 12, Fig. 14 and Fig. 16 respectively by 2.76%, 7.85% and 8.12%.

5. Conclusions

In the present work two procedures for automatic optimisation were presented. The first procedure allows to optimise a component shape thanks to the adjoint solution: at the computational cost of an additional solution, all the surface sensitivities with respect to one or a set of objective functions are obtained and can be used to generate a

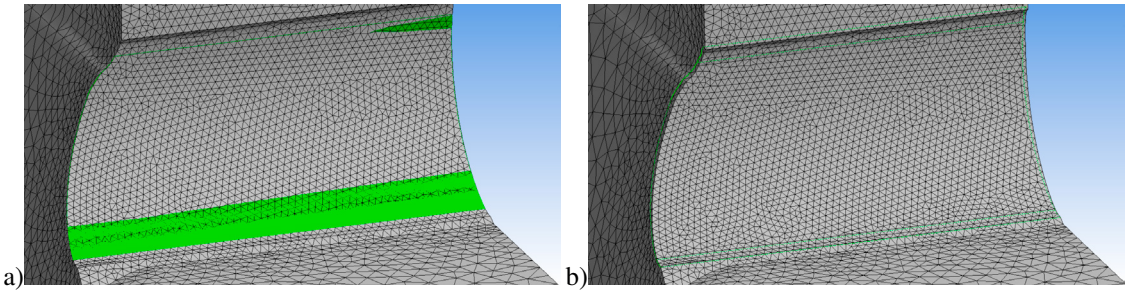

Fig. 11. Industrial component hotspot 1: a) baseline mesh configuration; b) optimised mesh configuration

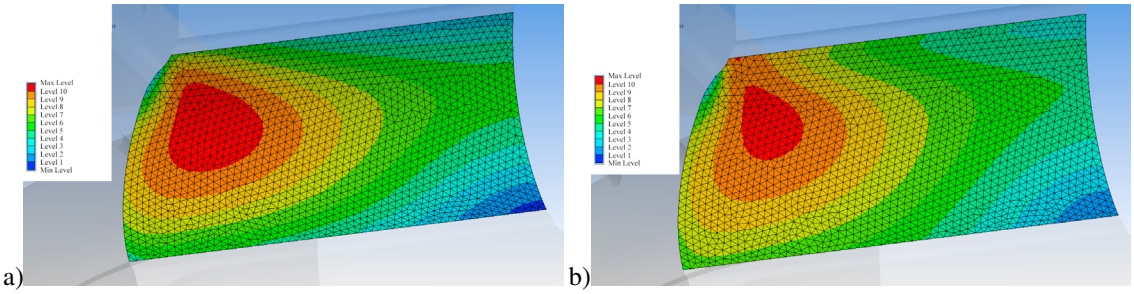

Fig. 12. Industrial component hotspot 1: a) baseline stress distribution; b) optimised stress distribution

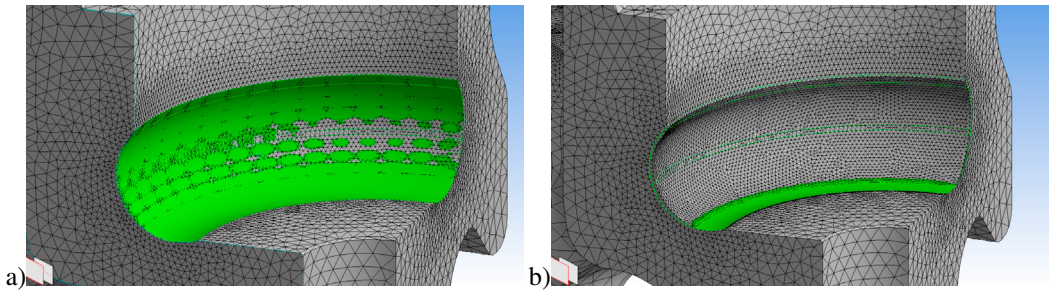

Fig. 13. Industrial component hotspot 2: a) baseline mesh configuration; b) optimised mesh configuration

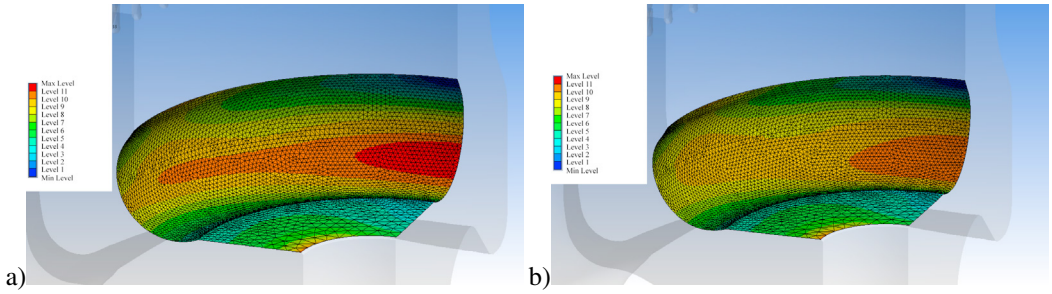

Fig. 14. Industrial component hotspot 2: a) baseline stress distribution; b) optimised stress distribution

sculpting function which moves nodes on the numerical model surfaces in the normal direction. The second procedure presented, based on the biological growth method, uses the surface stress levels to identify numerical model zones on which material can be added or removed and use this information to move in the normal direction, inward or outward, surface nodes. This procedure results in a stress peaks minimisation and in a more uniform distribution of

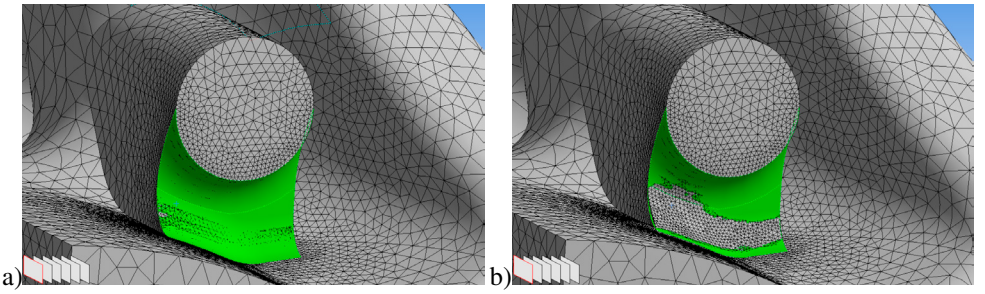

Fig. 15. Industrial component hotspot 3: a) baseline mesh configuration; b) optimised mesh configuration

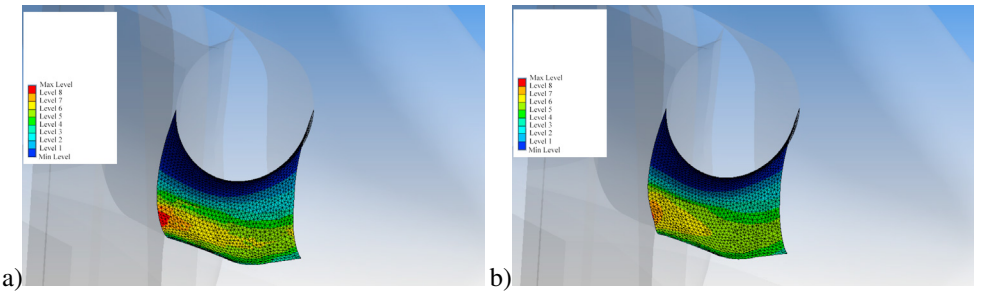

Fig. 16. Industrial component hotspot 3: a) baseline stress distribution; b) optimised stress distribution

stress levels in the component. These two approaches were successfully coupled with RBF based mesh morphing, in order to apply a displacement field on interested nodes according to data from adjoint and BGM procedure.

The proposed automatic workflows were first illustrated using a simple thick shell and then tested on a complex industrial component, on which different optimisation locations were identified. The proposed procedure allowed to reach optimised shapes matching different objective functions in an automatic way, with a minimal effort from the user. The framework adopted was composed by ANSYS® Workbench™ with RBF Morph™ ACT extension, which provided an integrated tool to the user in which perform optimisation task.

Acknowledgements

Authors would like to thanks ANSYS® for provided support to University of Rome “Tor Vergata” with the ANSYS Academic Multiphysics Campus Solution licenses, which were used to perform calculations described in this work.

References

Belegundu, A.D., 1985. Lagrangian Approach to Design Sensitivity Analysis. Journal of Engineering Mechanics 111, 680695. URL: http://ascelibrary.org/doi/10.1061/9399(1985)111:5(680).

Biancolini, M. E., Cella, U., 2010. An advanced RBF Morph application: Coupled CFD-CSM aeroelastic analysis of a full aircraft model and comparison to experimental data, 8th MIRA International Vehicle Aerodynamics Conference. Grove, United Kingdom.

Biancolini, M. E., 2011. Mesh morphing and smoothing by means of radial basis functions (RBF): a practical example using fluent and RBF morph, in “*Handbook of research on computational science and engineering: theory and practice*”, 2. IGI Global, Hershey PA, 347−380.

Biancolini, M. E., Groth, C., 2014. An efficient approach to simulating ice accretion on 2D and 3D airfoils. Advanced Aero Concepts, Design and Operations conference. Bristol, United Kingdom.

Biancolini, M. E., Chiappa, A., Giorgetti, F., Porziani, S., Rochette, M., 2018. Radial basis functions mesh morphing for the analysis of cracks propagation. Procedia Structural Integrity 8, 433−443.

Biancolini, M. E., 2018. Fast Radial Basis Functions for Engineering Applications, Springer, Berlin.

Biancolini, M. E., Chiappa, A., Giorgetti, F., Groth, C., Cella, U., and Salvini, P. 2018. A balanced load mapping method based on radial basis functions and fuzzy sets. International Journal for Numerical Methods in Engineering, 115(12), 1411-1429.

Brockman, R.A., Lung, F.Y., 1988. Sensitivity Analysis with Plate and Shell Finite Elements. International Journal for Numerical Methods in Engineering 26, 11291143.

Cella U., Groth C., Biancolini M.E., 2017. Geometric Parameterization Strategies for shape Optimization Using RBF Mesh Morphing, in "Advances on Mechanics, Design Engineering and Manufacturing". In: Eynard B., Nigrelli V., Oliveri S., Peris-Fajarnes G., Rizzuti S. (Eds). Springer, Cham. 537−545

Davies P. J., 1963. Interpolation and approximation, Blaisdell, London.

Dai, D. N., Hills, D. A., Hrkegard, G., & Pross, J. (1998). Simulation of the growth of near-surface defects. Engineering fracture mechanics, 59(4), 415-424.

de Boer, A., Van der Schoot, M.S., Bijl, H., 2007. Mesh deformation based on radial basis function interpolation. Computers & structures 85, 784−795.

Dems, K., Haftka, R.T., 1988. Two Approaches to Sensitivity Analysis for Shape Variation of Structures. Mechanics of Structures and Machines 16, 501522. URL: http://www.tandfonline.com/doi/abs/10.1080/08905458808960274, doi:10.1080/08905458808960274.

Dems, K., Mroz, Z., 1983. Variational approach by means of adjoint systems to structural optimization and sensitivity analysis-I. Variation of material parameters within fixed domain. International Journal of Solids and Structures 19, 677692. doi:10.1016/0020-7683(83)90064-1.

Francavilla, A., Ramakrishnan, C.V., Zienkiewicz, O.C., 1975. Optimization of shape to minimize stress concentration. The Journal of Strain Analysis for Engineering Design 10, 6370. doi:10.1243/03093247V102063.

Giorgetti, F., Cenni, R., Chiappa, A., Cova, M., Groth, C., Pompa, E., ... & Biancolini, M. E. (2018). Crack Propagation Analysis of Near-Surface Defects with Radial Basis Functions Mesh Morphing. Procedia Structural Integrity, 12, 471-478.

Groth, C., 2015. Adjoint-based shape optimization workflows using RBF. Ph.d thesis. University of Rome Tor Vergata. doi:10.13140/RG.2.2.33913.06245.

Groth, C., Chiappa, A., Biancolini, M. E., 2018. Shape optimization using structural adjoint and RBF mesh morphing. Procedia Structural Integrity 8, 379−389.

Groth, C., Cella, U., Costa, E., and Biancolini, M. E. (2019). Fast high fidelity CFD\CSM fluid structure interaction using RBF mesh morphing and modal superposition method. Aircraft Engineering and Aerospace Technology.

Heywood R. B., 1969. Photoelasticity for designers, Pergamon Press, Oxford.

Mattheck C., Burkhardt S., 1990. A new method of structural shape optimization based on biological growth. International Journal of Fatigue 12, 185−190.

Nadarajah, S.K., Jameson, A., 2001. Studies of the continuous and discrete adjoint approaches to viscous automatic aerodynamic shape optimization, in: 15th AIAA Computational Fluid Dynamics Conference, American Institute of Aeronautics and Astronautics, Reston, Virigina. doi:10.2514/6.2001-2530.

Newman, J., Taylor, A.C., 1999. Overview of sensitivity analysis and shape optimization for complex aerodynamic configurations. Journal of Aircraft 36. doi:arc.aiaa.org/doi/pdf/10.2514/2.2416.

Papoutsis-Kiachagias, E.M., Porziani, S., Groth, C., Biancolini, M.E., Costa, E., Giannakoglou, K.C., 2015. Aerodynamic Optimization of Car Shapes using the Continuous Adjoint Method and an RBF Morpher. EUROGEN 2015, 11th International Conference on Evolutionary and Deterministic Methods for Design, Optimization and Control with Applications to Industrial and Societal Problems , 115doi:10.13140/RG.2.1.1615.2165.

Papoutsis-Kiachagias, E., Andrejasic, M., Porziani, S., Groth, C., Erzen, D., Biancolini, M., Costa, E., Giannakoglou, K., 2016. Combining an RBF-based morpher with continuous adjoint for low-speed aeronautical optimization applications, in: ECCOMAS Congress 2016 - Proceedings of the 7th European Congress on Computational Methods in Applied Sciences and Engineering.

Porziani, S., Groth, C., Biancolini, M. E., 2018. Automatic shape optimization of structural components with manufacturing constraints. Procedia Structural Integrity 12, 416−428.

Staten, M. L., Owen, S. J., Shontz, S. M., Salinger, A. G., Coffey, T. S., 2011. A comparison of mesh morphing methods for 3D shape optimization, 20th international meshing roundtable. Paris, France.

Waldman W., Heller M., 2015. Shape optimization of holes in loaded plates by minimization of multiple stress peaks. Technical Report, Defence Science and Technology Organisation Fisherman Bend, Australia, Aerospace Div, Apr. 2015.

Yatheendhar, M., Belegundu, A.D., 1993. Analytical shape sensitivity by implicit differentiation for general velocity fields. Computers and Structures 46, 617623. doi:10.1016/0045-7949(93)90390-Y.